









Article

Application of Severe Weather Nowcasting to Case Studies in Air Traffic Management

Laura Esbrí ^{1,*}, Tomeu Rigo ², María Carmen Llasat ¹, Riccardo Biondi ³, Stefano Federico ⁴, Olga Gluchshenko ⁵, Markus Kerschbaum ⁶, Martina Lagasio ⁷, Vincenzo Mazzarella ⁷, Massimo Milelli ⁷, Antonio Parodi ^{7,*}, Eugenio Realini ⁸ and Marco-Michael Temme ⁵

- ¹ Department of Applied Physics, University of Barcelona, 08028 Barcelona, Spain; mcarmenllasat@ub.edu
² Meteorological Service of Catalonia, 08017 Barcelona, Spain; tomeu.rigo@gencat.cat
³ Dipartimento di Geoscienze, Università degli Studi di Padova, 35122 Padova, Italy; riccardo.biondi@unipd.it
⁴ National Research Council of Italy, Institute of Atmospheric Sciences and Climate (CNR-ISAC), 00133 Rome, Italy; s.federico@isac.cnr.it
⁵ German Aerospace Center (DLR), 38108 Braunschweig, Germany; olga.gluchshenko@dlr.de (O.G.); marco.temme@dlr.de (M.-M.T.)
⁶ Austro Control, 1030 Vienna, Austria; markus.kerschbaum@austrocontrol.at
⁷ CIMA Research Foundation, 17100 Savona, Italy; martina.lagasio@cimafoundation.org (M.L.); vincenzo.mazzarella@cimafoundation.org (V.M.); massimo.milelli@cimafoundation.org (M.M.)
⁸ Geomatics Research & Development srl (GReD), 22074 Lomazzo, Italy; eugenio.realini@g-red.eu
* Correspondence: lesbri@meteo.ub.edu (L.E.); antonio.parodi@cimafoundation.org (A.P.)

Abstract: Effective and time-efficient aircraft assistance and guidance in severe weather environments remains a challenge for air traffic control. Air navigation service providers around the globe could greatly benefit from specific and adapted meteorological information for the controller position, helping to reduce the increased workload induced by adverse weather. The present work proposes a radar-based nowcasting algorithm providing compact meteorological information on convective weather near airports for introduction into the algorithms intended to assist in air-traffic management. The use of vertically integrated liquid density enables extremely rapid identification and short-term prediction of convective regions that should not be traversed by aircraft, which is an essential requirement for use in tactical controller support systems. The proposed tracking and nowcasting method facilitates the anticipation of the meteorological situation around an airport. Nowcasts of centroid locations of various approaching thunderstorms were compared with corresponding radar data, and centroid distances between nowcasted and observed storms were computed. The results were analyzed with Method for the Object-Based Evaluation from the Model Evaluation tools software (MET-10.0.1, Developmental Testbed Center, Boulder, CO, US) and later integrated into an assistance arrival manager software, showing the potential of this approach for automatic air traffic assistance in adverse weather scenarios.

Keywords: weather radar; storm; nowcasting; adverse weather; convective cells; air traffic control; air traffic controller support; severe weather



Citation: Esbrí, L.; Rigo, T.; Llasat, M.C.; Biondi, R.; Federico, S.; Gluchshenko, O.; Kerschbaum, M.; Lagasio, M.; Mazzarella, V.; Milelli, M.; et al. Application of Severe Weather Nowcasting to Case Studies in Air Traffic Management. *Atmosphere* **2023**, *14*, 1238. <https://doi.org/10.3390/atmos14081238>

Academic Editor: Michael L. Kaplan

Received: 20 June 2023

Revised: 28 July 2023

Accepted: 28 July 2023

Published: 1 August 2023



Copyright: © 2023 by the authors. Licensee MDPI, Basel, Switzerland. This article is an open access article distributed under the terms and conditions of the Creative Commons Attribution (CC BY) license (<https://creativecommons.org/licenses/by/4.0/>).

1. Introduction

Severe weather (large hail, straight-line convective winds, or tornadoes), along with other adverse weather (e.g., heavy rainfall, fog), has a notable impact on air traffic operations. These phenomena cause critical delays and other flight impacts, mainly during days with a large volume of operations [1]. For instance, Munich airport was affected by thunderstorms on more than 9% of days during the first half of 2018. At Frankfurt/Main airport, 45% of delays in 2010 were caused by adverse weather [2]. In the first half of 2018, weather was responsible for 8.3% of all flight delays in Europe [2]. According to the United States Air Force [3], pilots have two options when they are facing severe thunderstorms:

either diverting to the closest unaffected area by traversing the thunderstorms or bypassing them. This decision should be taken quickly to ensure flight safety.

Weather radars have become very beneficial for identifying, tracking and nowcasting thunderstorms and their associated meteors (severe weather or heavy rainfall). The main advantages are spatial and temporal resolutions on the order of 1 km^2 and 5 min, respectively [4,5]. These scales are compatible with those associated with the resolution of severe weather phenomena [6]. The main disadvantages are the large amount of information from weather radar volumes, in addition to possible errors and non-meteorological echoes that may appear [7–9]. Quick decision-making, such as is required in aircraft landing and take-off maneuvers, requires optimization of these data as well as of processes for the identification, monitoring, and prediction of convective danger zones.

There are many real-time operational products that provide partial or complete information about the atmospheric volume surrounding a weather radar. These are divided into two categories. The first yields information for a single atmospheric level; the most common products are the plan position indicator (PPI) and constant altitude PPI (CAPPI). The PPI provides the reflectivity field at a constant elevation (angle regarding the horizontal of the place) of the radar antenna. The CAPPI includes interpolated data at a constant altitude (e.g., [10]). The vertical analysis of CAPPI products allows it to identify 3D structures that usually are called “cells”. In contrast, vertically integrated liquid (VIL) and VIL density or DVIL (VIL divided by the echo top of the reflectivity volumetric fields, which may be equivalent to a normalized VIL) products provide detailed atmospheric information of the entire volume [11]. They integrate the reflectivity of a column with height, but cannot distinguish the contribution of each level.

The first radar nowcasting techniques were summarized in [12]. Most of them are based on the identification of precipitating systems in two dimensions or cells in three dimensions and perform the nowcasting by extrapolating the trajectories followed by these 2D or 3D systems (e.g., [13–15]). Subsequently, these techniques have been improved by introducing the wind field (i.e., [16]), integrating it with meteorological models by blending (i.e., [17]), or taking into account possible anomalous movements (i.e., [18]). Among these methodologies are the well-known 3D multi-threshold nowcasting systems such as TITAN [13], SCIT [14], and CORTEC [15]. New ways have recently emerged of improving the capabilities of the traditional methods using artificial intelligence [19,20] or statistics [21,22].

However, these technologies are currently not yet applicable to air traffic management (ATM) due to its complexity and the type of fast and simple product needed to feed ATM models and help air traffic controllers and pilots make decisions. In [23], the authors presented an example of a civil aviation problem and the capabilities of weather radar for providing favorable solutions to air-traffic managers in complicated situations caused by severe weather. They illustrated the complexity of providing concise information to end-users, mainly because of the difficulty of obtaining accurate thunderstorm forecasts and the time required to process the information.

The present paper proposes a nowcasting algorithm that offers simplified storm information considering radar volumetric data using DVIL products and a centroid-based nowcast strategy. This algorithm has been developed and tested in the context of the project “Satellite-borne and IN situ Observations to Predict The initiation of Convection for Air traffic management” (SINOPTICA). It is focused on the prediction of severe weather areas that may be dangerous for aviation and its integration into Arrival Managers (AMANs). AMANs are developed and operationally used for Air Traffic Control (ATC) assistance. The project’s target was the fast and reliable prediction of severe weather areas for integration into extended arrival management system to support air traffic controllers guiding aircraft during approach phase. The early determination of an arrival sequence on the bases of the current and forecasted operational situation increases predictability for all involved processes, resulting in increased cost-efficiency for all stakeholders (air navigation service providers, airlines, airports, etc.). Increased punctuality enables more efficient airline

management and increases passenger satisfaction. Efficient arrival management decreases airborne arrival delays; thus, at the same time, it significantly decreases environmental impacts (e.g., CO₂, soot, noise). Timely consideration of weather impacts de-complexifies the incoming traffic, reduces air traffic controller workload, and consequently increases safety. An extended AMAN allows ATC to calculate the arrival sequence and the corresponding arrival times well in advance with routing advisories depending on the predicted convection behavior [24]. This sequencing software runs in real time and needs weather information for up to 30 min ahead of the current time. Because the weather radar observations are already outdated by the time they have been processed, one of the challenges of the project was to ingest precise weather nowcasts with minimal computing time.

2. Data

The principal data were various weather radar products from the Italian radar mosaic managed by Italian Civil Protection [25]. The data format was GeoTIFF. Each product has temporal and spatial resolutions of 5 min and 1 × 1 km, respectively. The radar products used were:

- CAPPI: reflectivity fields at a certain height (1 km, 3 km and 5 km CAPPIs were available) interpolated from PPI elevations. It is a good indicator of rainfall intensity.
- VIL: Product equivalent to the total amount of water available on a vertical column of the atmosphere. Large values indicate either large hail occurrence, large amounts of small hail, or very high rainfall intensity.
- ETM (echo top maximum): Corresponds to the maximum height at which there is a minimum reflectivity intensity of 20 dBZ. It is a good indicator of the top of storm clouds.
- DVIL: This incorporates ETM information to the VIL product, making it a better severe weather indicator with less dependence on seasonality, as it normalizes the height of the precipitable column (see, e.g., [26] for more information). This is a derived product, and is not directly calculated by the radar software. It can be obtained using Equation (1). Thus, thunderstorms may be compared and analyzed in terms of their severity with less seasonal dependence. The utility of this product makes even more sense if works such as [23] are considered. They concluded that VIL and ETM can aid ATC in route operations into the US.

$$\text{VIL density} \left[\frac{\text{g}}{\text{m}^3} \right] = \frac{\text{VIL}}{\text{ETM}} \quad (1)$$

The two other data types used were ground observations of severe weather from the European Severe Weather Database (ESWD, [27]) and real aircraft trajectories from FlightRadar24 around the regions of interest for the cases study. The ESWD observations were used to analyze DVIL products performance. FlightRadar24 collects Automatic Dependent Surveillance—Broadcast (ADS-B) data from satellite aircraft data from commercial and private ADS-B receiving stations, synchronizes these data, and makes them available as raw data. Before using the raw data, trajectories are time-mapped and filtered with respect to place rounds of paratroopers, military aircraft, and helicopters. These trajectories were used as traffic scenarios to compare the performance of the AMAN software before and after integrating the meteorological nowcasts.

The weather radar fields consider the distance of each mapped pixel to the closest airport to determine the impact of severe weather at Italian airports. Figure 1 shows the principal regions of interest (red areas), with distances < 50 km from the airports covered by the Italian radar mosaic. The ATC landing and take-off operations take place in these regions. Due to their higher air traffic density and more complex meteorology, the regions of northern Italy and Rome were of particular interest.

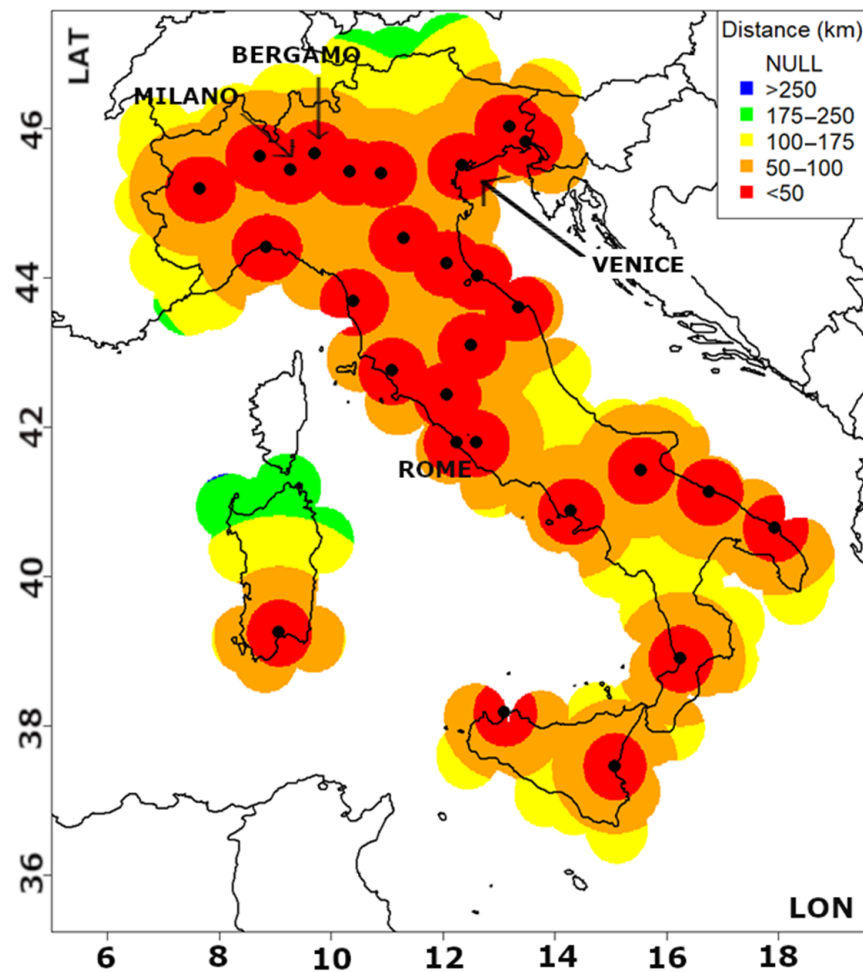


Figure 1. Map showing principal Italian airports (black points) with regions of interest according to the above legend color scale. Colors are assigned according to distance between the radar composite field and the nearest airport. For example, red areas indicate distances ≤ 50 km, with orange areas indicating 50–100 km and yellow ones 100–175 km.

3. Methodology

The objective of this study was to develop a decision support tool that can be operational in ATC to assist pilots in their approach to an airport while avoiding areas of convective hazard. To achieve this, the nowcasting algorithm aims to anticipate regions where intense storms may occur in order to provide alternative routes through an extended Arrival Manager (AMAN) [24]. First, the system must determine the presence or absence of storms near the airport (within a radius of 150 nautical miles, approx. 277 km). In case there are active storm cells, it must ascertain the timestamp, position of the centroid of each storm cell, its area, and the direction of its movement, along with their nowcasting for the next 10 min. The AMAN runs continuously, with meteorological information updated every 10 min.

This section describes in more detail the steps of the methodology used to perform the nowcasting. The proposed methodology is based on previous techniques [13,18,28], but considers DVIL instead of using reflectivity fields or VIL, as most algorithms found in the literature do [29,30]. Although cell extent and shape are not as well-defined as in certain well known 3D algorithms already in use for standard forecasting [13–15], the developed tool has the potential to be faster without losing much in terms of prediction accuracy.

The main rationale for this selection is the favorable performance as a descriptor of the vertical atmospheric column and decreased run time of the algorithm. The VIL Density is capable of summarizing with high efficiency the information from the radar

volume in a single 2D field. It allows us to only focus on the most intense parts of the storms (exceeding 45 dBZ for the reflectivity values and reaching at least 30 dBZ at higher levels [18,31]) without the need to analyze reflectivity values at different vertical levels. Previously implemented algorithms had to analyze whether or not reflectivity thresholds are exceeded at different vertically levels in order to characterize storms. Additionally, to identify convective storms, they demand a certain reflectivity intensity at a specific height.

In addition, in the context of the specific application of this study, the determination of the altitude where there is the most intense part of the storm, that is, analysis of the vertical structure, yields limited added value. The software into which the outputs are to be integrated is designed only to assist during the approach phase of the aircraft to the airport, which primarily occurs at low altitudes. During this critical phase, the feasibility of flying over or under a storm is often impractical. Therefore, the selection of the DVIL as the variable of focus contributes to maintaining a low level of complexity, thereby increasing the time efficiency, which is a crucial aspect for real-time applications when considering a large area and having short decision times. The entire procedure has been branded the RaNDeVIL algorithm (Radar Nowcasting with Density of VIL).

3.1. Identification and Characterization of Storm Structures

Previously, to perform nowcasting of storms algorithm performed a storm characterization. This implies the identification of all cells constituting the storm. The configuration of each individual convective structure is defined according to R_i (minimum intensity threshold for the chosen weather radar variable) and R_s (minimum size to consider as a storm cell). In this case, these thresholds were adjusted to identify and nowcast convective episodes (hail, heavy rainfall, and strong winds) that might compromise flight safety or normal airport operations. The first experiments with the proposed algorithm for the study cases of the SINOPTICA project were configured with $R_s = 10$ pixels (spatially contiguous pixels, building a storm structure of at least 10 km^2) and four R_i thresholds of DVIL value exceedance: 0.5, 1, 1.5, and 2.5 g/m^3 . The spatial threshold was selected to be consistent with previous characterizations of Mediterranean convective storms, following [32]. The tested DVIL thresholds have been decided according to the expertise of the Meteorological Service of Catalonia, considering the target of this study, to identify potentially severe storms in a Mediterranean area; Refs. [33,34] showed that in the Mediterranean area, hail may occur from relatively low DVIL values (typically $> 1 \text{ g/m}^3$). The results in this report only consider $R_i = 1 \text{ g/m}^3$, which shows the better ability to reproduce the lifecycle of the storms in the analyzed study cases. With a less restrictive threshold (lower), there were too many cells merging and splitting continuously, and the life cycle was interrupted. With a threshold above 1 g/m^3 , the number of identified cells drastically decayed; cells were only spotted once in their entire cycle of life, or only appeared in very short time intervals.

The first steps shown in Figure 2 illustrate the storm identification process of the algorithm. When the region of interest (ROI) is defined, the DVIL product is calculated for each time step in order to facilitate data ingestion. A new raster file is generated containing groups (clumps) of at least R_s pixels (10 in this case) exceeding a selected R_i threshold. Each group is identified as a storm cell, and a numerical value is assigned as a label (Process 1, Figures 2 and 3). This label allows the individual tracking (Process 2, Figures 2 and 3) and nowcasting (Process 3, Figures 2 and 3) of the storm cells. For each storm cell and step of time, the following information is stored in a CSV file: date (yyyymmdd) and hour (hhmm, UTC), longitude and latitude of the storm centroid (calculated as an intensity-weighted average of all latitudes and longitudes of the pixels grouped in the storm cell), area (number of 1-km^2 pixels), and maximum, minimum, and mean values of radar (VIL, ETM, and DVIL). This file, as well as the different 'csv' files with the nowcasting information of the identified storm cells, make up the outputs of the algorithm.

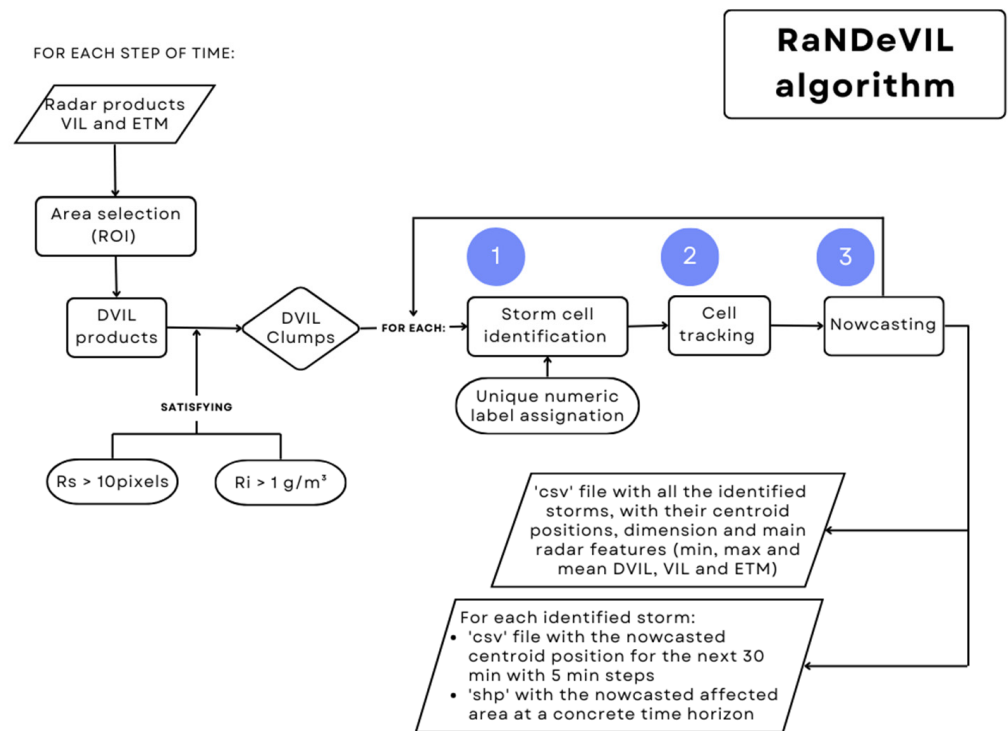


Figure 2. Flux diagram for the RaNDeVIL algorithm applied to the different case studies. The numbers 1–3 indicate the processes to be repeated for each one of the storms identified in the DVIL raster file with the defined clumps.

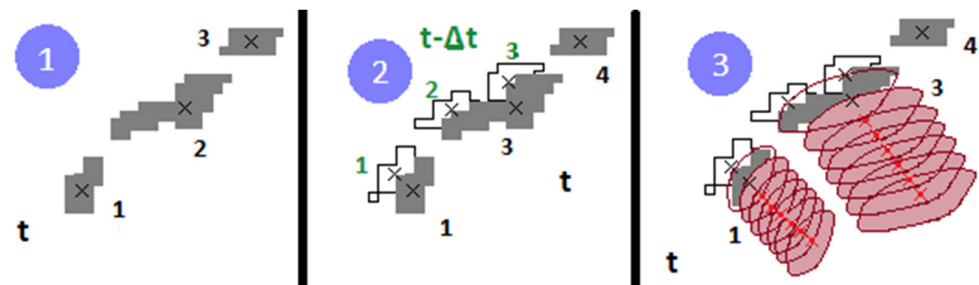


Figure 3. Graphical scheme of Processes 1–3 (inside blue circles) at a given time step (t). 1. The storms are identified (grey shaded, the cross identifies the centroid position), with the initial numeric labels assigned (numbers in black). 2. The previous radar image is used to identify the storms already existing in the previous time step (contours, labels in green), and the labels are corrected (new labels in black). 3. For those storms that were identified in at least at two time steps, the nowcasted centroid positions are calculated (red crosses) and the storm area is fitted into an ellipsoid and then extrapolated to represent the area expected to be affected according to the nowcast of the centroids (wine red).

3.2. Tracking

The objective in the tracking part is to be able to follow a storm cell, ideally through its entire lifecycle, i.e., its development, growth, and decay stages. What makes this challenging is the various splitting or merging processes that a storm cell may undergo during its lifecycle. As mentioned, we only consider thunderstorms in 2D. In this approach, a storm cell is tracked (Figures 2 and 3, Process 2) using the assigned labels in the prior step. The information from the prior radar DVIL product is used to correct the assigned labels if the identified storms already existed in that previous time step. This step allows us to obtain the tracking of the storm. The evolution of the storm is followed while there is an

overlapping area of DVIL exceeding the R_i threshold (1 g/m^3 for the results shown in this study) during two consecutive time steps (5 min steps).

At the end of the procedure, for each combination of R_i and R_s the algorithm generates a text file containing all relevant information of the storm cells identified and tracked during an episode.

3.3. Short-Term Nowcasting

When a storm cell exists for at least two consecutive time steps (10 min in our case), future locations of the storm centroid can be nowcasted (Figures 2 and 3, Process 3). The equations used to forecast the future location of the storm cells are similar to other centroid base nowcasting methods (i.e., [13]). They use the past locations of the storm centroid to lineally extrapolate the future locations for the next time steps. The following equation provides the predicted centroid coordinates for a single storm cell (a_F):

$$a_F = a_0 + a_1 \cdot h_t \quad (2)$$

where h_t is the number of 5 min intervals from the last observation ($h_t = 1$ means a nowcast horizon of 5 min and $h_t = 12$ means $12 \times 5\text{-min} = 60\text{-min} = 1 \text{ h}$). Equations (3) and (4) describe a_0 and a_1 coefficients respectively, where n is the number of 5 min intervals the cell has been observed at in the previous images (observations until time i), x_i is the longitude or latitude at i , and tt_i is the corresponding term in the sequence of tracking ($-n + 1, -n + 2, \dots; 0$).

$$a_0 = \frac{\sum_{i=0}^n x_i \cdot \sum_{i=0}^n tt_i^2 - \sum_{i=0}^n tt_i \cdot \sum_{i=0}^n (x_i \cdot tt_i)}{n \cdot \sum_{i=0}^n tt_i^2 - (\sum_{i=0}^n tt_i)^2} \quad (3)$$

$$a_1 = \frac{2}{3} \frac{n \cdot \sum_{i=0}^n (x_i \cdot tt_i) - \sum_{i=0}^n tt_i \cdot \sum_{i=0}^n x_i}{n \cdot \sum_{i=0}^n tt_i^2 - (\sum_{i=0}^n tt_i)^2} \quad (4)$$

By applying these equations to longitude and latitude coordinates, a pair of motion vectors with forecast coordinates are obtained, showing predicted locations for a storm cell in steps of 5 min. The storm area from the last DVIL product is adjusted to an ellipsoid and then used to extrapolate the nowcasted area to be affected by the storm.

3.4. Analysis of Results

The process of analysis involved three steps. The first consisted of a qualitative analysis of the thunderstorms associated with severe weather cases selected and discussed within the SINOPTICA project. To accomplish this, individual tracked and nowcasted storms were obtained with RaNDeVIL. The second step is a quantitative evaluation performed with the Method for the Object-Based Evaluation (MODE, [35]) from the Model Evaluation Tools software (MET-10.0.1, Developmental Testbed Center, Boulder, CO, USA) [36,37]. This evaluation was applied to the RaNDeVIL output files that were selected for integration into the ATM software (4-dimensional Cooperative Arrival Manager, German Aerospace Center (DLR), Braunschweig, Germany). The MODE identifies the spatial structures (objects) and computes for each of them the following attributes: centroid distance, angle difference, symmetric difference, and percentile intensity. These attributes were used as input to a fuzzy logic engine that performed the matching and merging steps and summarized the attributes into a single value called the total interest [38]. The score ranges from 0 to 1, with 1 being the best score. Finally, in the third step, the integrated nowcasting outputs for one case study were displayed in the software to assist the air traffic controllers in organizing the air traffic around a storm system to corroborate its usability.

4. Case Studies

The defined ROI covers the northern Italian peninsula (6.1° E to 14° E ; 43° N to 47.4° N) and includes three severe weather events that affected the normal operation of three major Italian airports in 2019. Figure 4 summarizes the main hazards for each case

study in the vicinities of the airports and the DVIL fields at the time when the impact on the airports was the greatest.

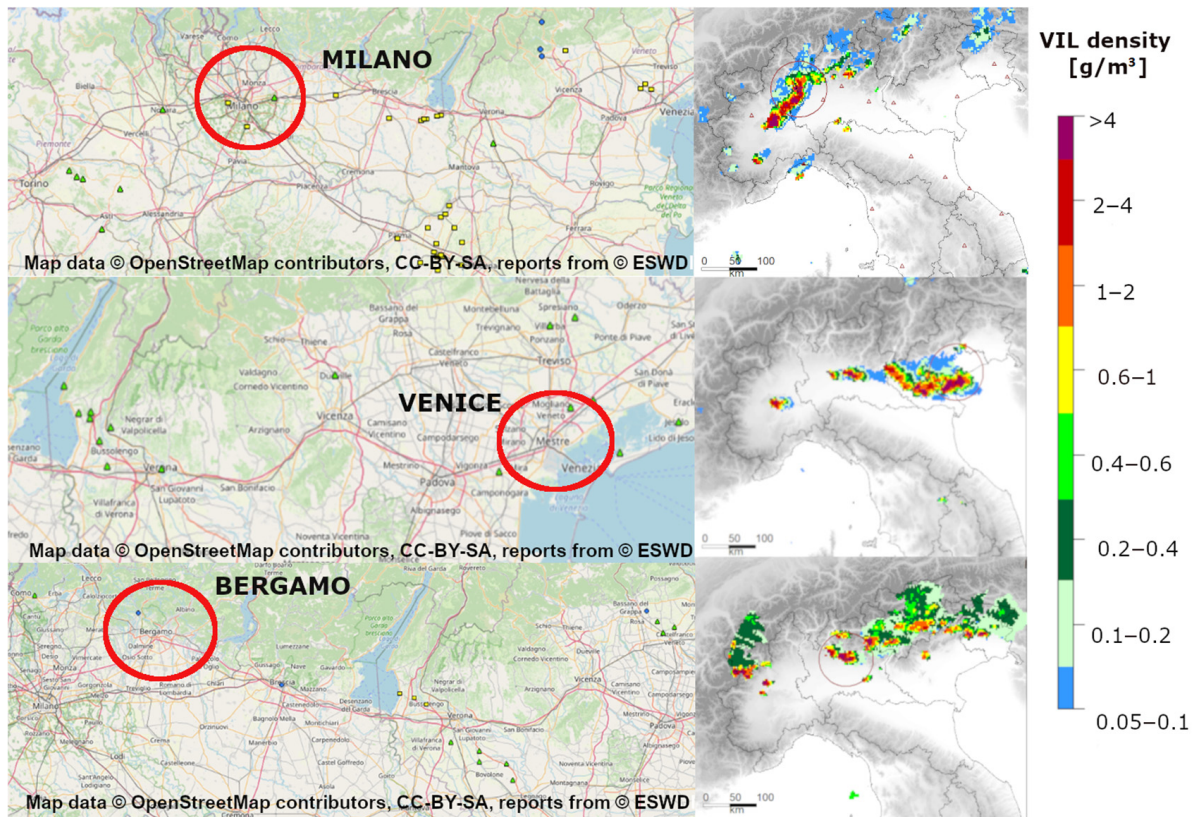


Figure 4. Left: Maps with ground records of severe weather (green triangle for large hail, blue dots for heavy rain, and yellow squares for severe wind) from the ESWD database of the European Severe Storms Laboratory (Map data © OpenStreetMap contributors, CC-BY-SA, reports from © ESWD) for the three selected events: 5 May 2019 Milano-Malpensa (**top**), 7 July 2019 Venice (**middle**) and 6 May 2019 Bergamo (**bottom**). Right: DVIL fields at the time of major impact at each airport (designated by red circles).

The first event was on 11 May 2019, and was characterized by the development of a squall line crossing the Malpensa airport between 14 and 15 UTC [39]. The large hail amounts on the runways combined with frequent lightning and strong winds caused flight delays of nearly two hours. In addition, air traffic controllers had to divert nine aircraft to other airports.

The second case was a very intense rainfall on 7 July 2019 impacting the Venice region. The rainfall was accompanied by a sandstorm, hail, and strong winds (60–70 km/h) in different areas and a downburst in the vicinity of Venice airport. Again, eight aircraft had to be diverted to other airports.

The third episode took place during the night of 6 August 2019, mainly affecting the secondary airport of Bergamo, Orio al Serio. In this case, 120.8 mm of accumulated precipitation was registered in 24 h at Almenno San Salvatore (near Bergamo airport), along with wind gusts of ~59.5 km/h. Consequently, seven flights were diverted to other airports and departing aircraft experienced significant delays.

Maps of the maximum daily DVIL were compared with the places where large hail or severe wind was recorded (Figures 5 and 6). For the set of ground data in each of the three cases, the maximum DVIL within a buffer area around the observation (to reduce uncertainty, a circumference of radius 25 km was used) varied mainly between 6.0 and 10.5 g/m^3 , while the mean DVIL in the same buffer area was between 1.0 and 2.8 g/m^3 .

The studied cases with observed large hail have greater DVIL values (maxima between 8.0 and 10.5 g/m³ and means between 1.9 and 2.9 g/m³) than those characterized by severe wind (maxima between 5.0 and 10.6 g/km³ but means between 0.6 and 1.4 g/km³). These differences are a consequence of a stronger correlation between radar values and hail than between those values and wind.

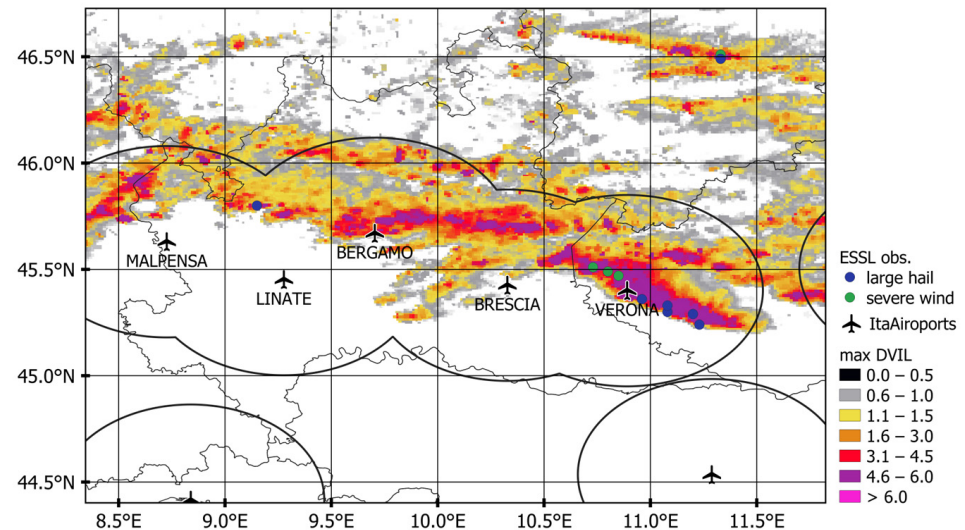


Figure 5. Maps of daily maximum DVIL with ESSL observations for the case of 6 August 2019. Black circular lines delimit areas within $d \leq 50$ km of an Italian airport.

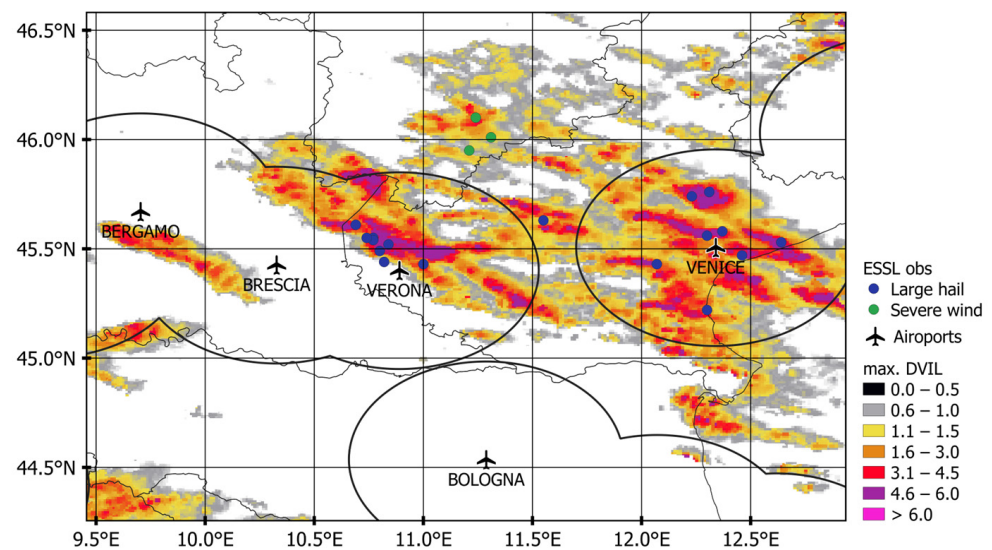


Figure 6. Same as Figure 5 for the case of 7 July 2019.

5. Results

5.1. Individual Tracking and Nowcasting of Storm Cells for the Three Events

The focus of this section is to evaluate the ability of the algorithm to provide relevant information to the end user (ATM staff) in decision-making situations with severe weather. Figures 7–9 show the evolution of convective storms at different times to illustrate the main issues involving ATM. In all cases, as discussed in the methodology (Section 3.1), the imagery shows the results for $R_s = 10$ (10 km²) and R_i (DVIL) = 1.0 g/m³.

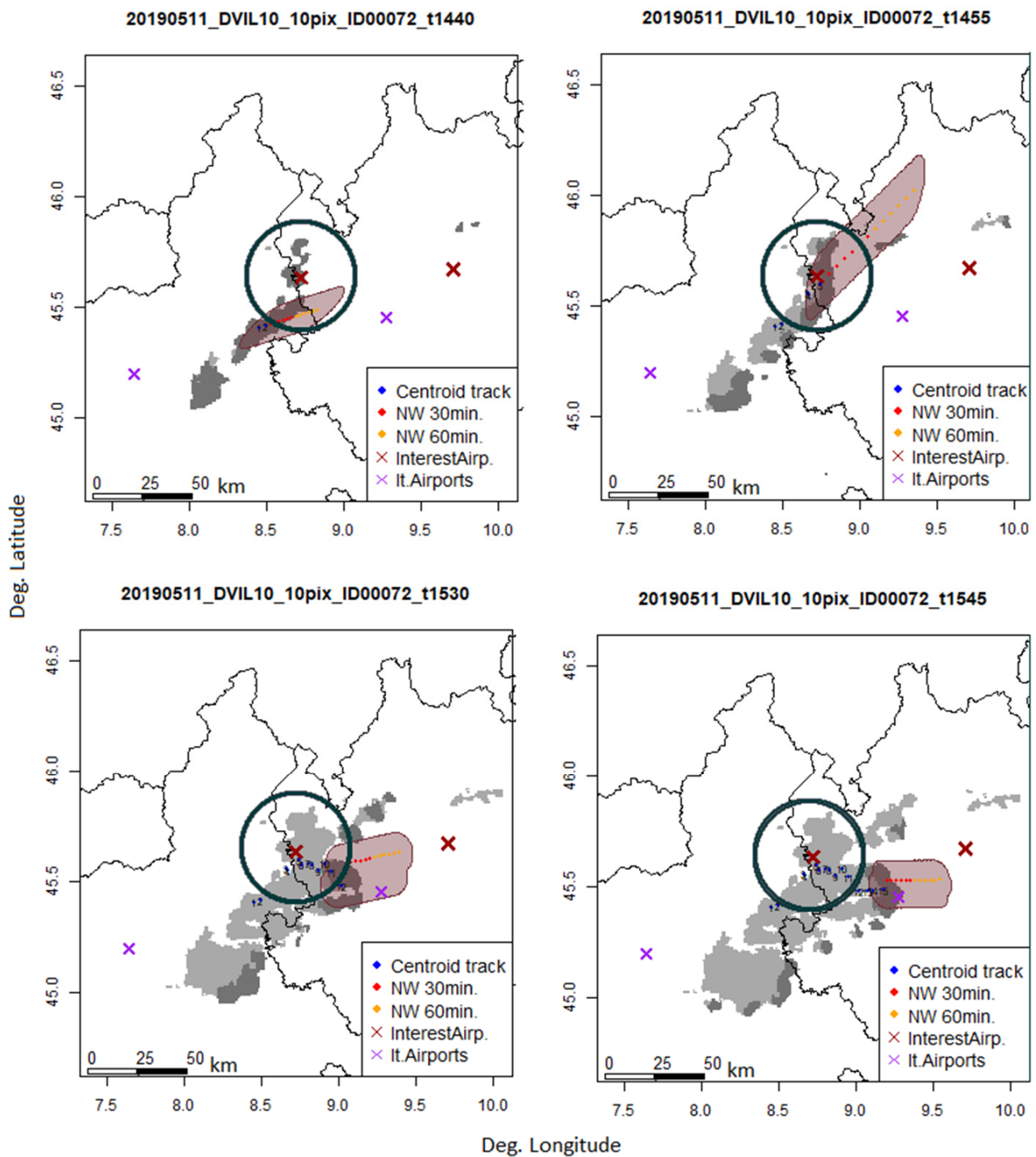


Figure 7. Various nowcasting outputs at 14:40, 15:00, 15:20, and 15:40 UTC for the storm cell ID00072 (ID72) during the event of 11 May 2019 (Milano-Malpensa airport). Dark grey-shaded areas indicate current cell locations, while light grey-shaded areas are previously affected areas. The numbered blue dots are already-observed locations of the storm centroid (tracking), and red and orange dots are nowcast locations for the subsequent 30–60 min (in 5 min steps). The wine translucent area corresponds to the area predicted to be affected by the storm for the next 60 min. Red crosses show the airports of interest, and purple crosses correspond to secondary airports. The green circle delimits the considered area of operations (50 km radius).

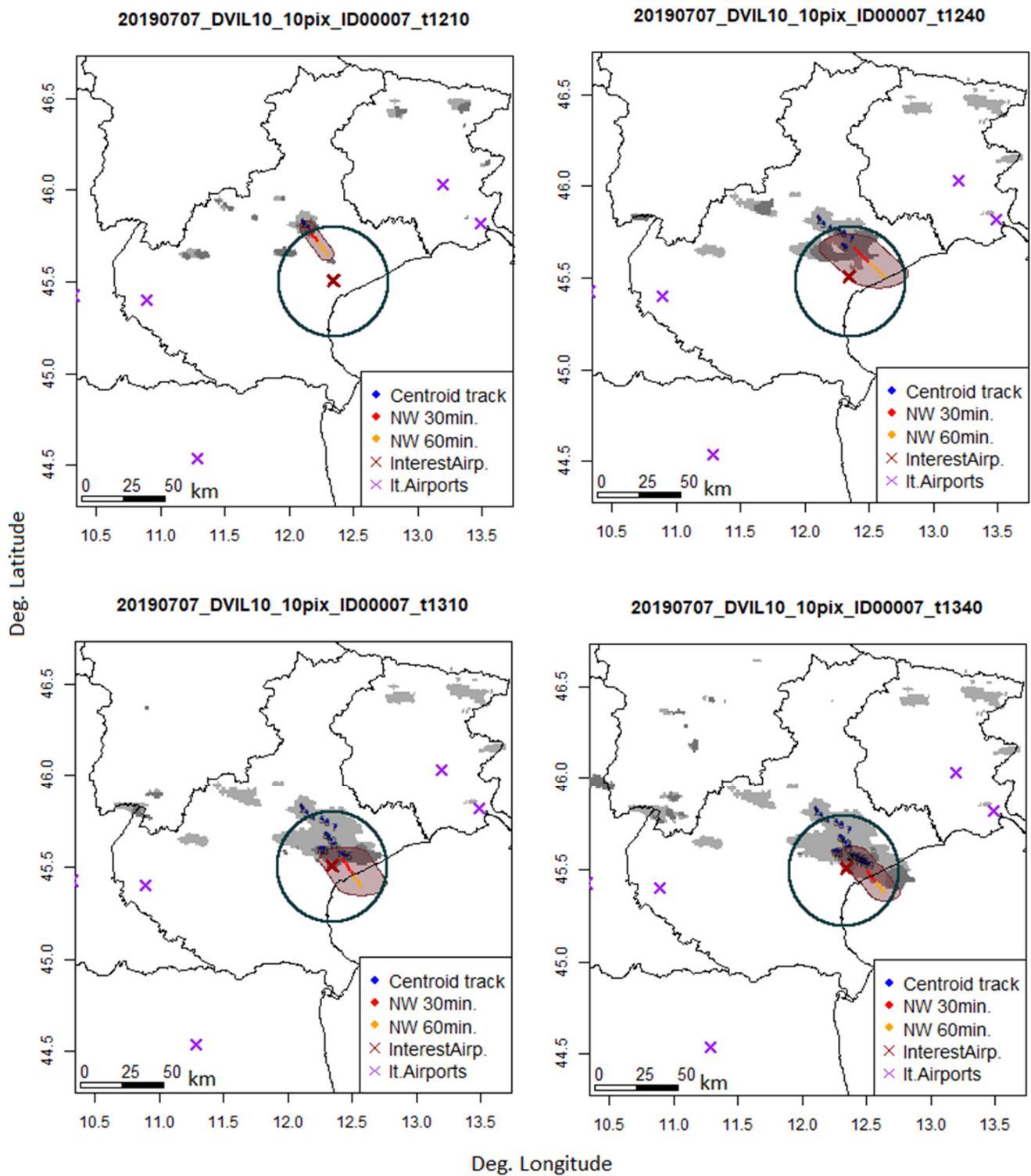


Figure 8. Same as Figure 7 for storm cell ID00007 (ID7), which affected Venice Airport during 7 July 2019, at 12:10, 12:40, 13:10, and 13:40 UTC.

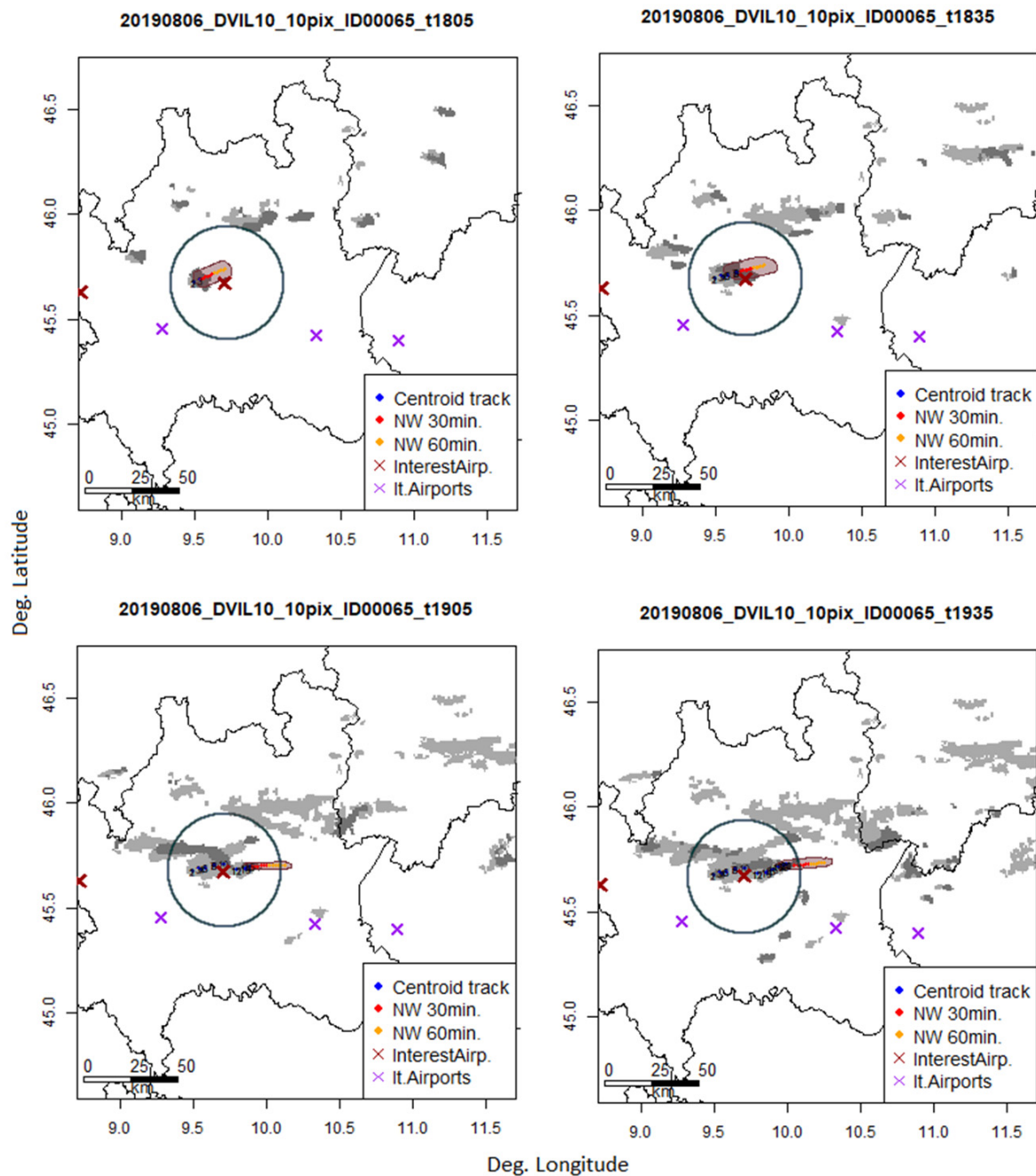


Figure 9. Same as Figure 7 for Bergamo Airport, 6 August 2019, cell labelled with ID00065 (ID65), at 18:05, 18:35, 19:05, and 19:35 UTC.

5.1.1. Milano Case, 11 May 2019

On 11 May 2019, a large hailstorm struck Milano-Malpensa airport. The event was characterized by a long quasi-linear system that moved from west to east, crossing nearly all of northern Italy, that included various interacting convective cells. Despite the large size of the convective system, the different interacting convective cells underwent multiple splitting and merging processes, complicating the nowcasting process (Section 4). The area of operations of the airport (a 50 km radius around the airport) was affected by the storms for more than an hour between 14:00 and 16:00. As an example, Figure 7 shows the nowcasting of cell ID72, illustrating the evolution of the ID72 cell storm from 14:40 to 15:40 UTC. The storm lived until 17:35 UTC; however, the target of Figure 7 is to estimate the end time of the warning situation for the airport considering the area of operations.

The DVIL radar products (observations) indicate that the end-time for the airport being affected was 15:45 UTC, more than one hour after event initiation. Due to the typical highly convective nature of severe thunderstorms, this is a very long period. It can be observed that at 14:40 the airport was already affected by a smaller cell that merged with ID72 around 14:50 UTC. At 15:00 UTC, the algorithm already provides a good forecast of the end of the danger period in the area of operations in about 40 min (15:40 UTC). However, the forecasted direction of propagation for the storm at that time was not accurate because of a merger that occurred 10 min before this forecast. The nowcasted storm trajectory improves in the following time steps, although another merging at 15:25 again changes the propagation direction.

5.1.2. Venice Case, 7 July 2019

In this second case (7 July 2019), a severe thunderstorm affected Venice airport and its surroundings. Figure 8 compares nowcast and radar-observed data in 30 min steps near the airport, showing the evolution of the storm ID7 from 12:10 to 13:40 UTC. According to the radar images, at 13:10 UTC the storm was over the airport.

The algorithm successfully located up to five cells in the vicinity from one hour before this occurrence, when the centroid locations were starting to approach the area of influence for landing/departure operations. At 12:10 UTC, storm ID7 was 52 km northwest of the airport (Figure 8). One of the strengths of the algorithm is correct forecasting of the translating direction, although the nowcasted area had poor accuracy, expecting the cell to move faster than it actually did. Thirty minutes later the analyzed cell merged with a minor one located south of the airport that was moving from west to east. The merger did not affect either cell translation or nowcasting, which continued to indicate a similar trajectory for the larger structure, just as before but with increased area. After this merging, the direct impact on the airport and its surroundings was confirmed. At 13:10 UTC, the thunderstorm entirely covered the airport (with its centroid 11 km northwest) and had already reached maturity (implying that the probability of occurrence of severe weather was greater than at any other time). From 13:10 to 13:40 UTC, the thunderstorm split. A portion of the storm cell remained quasi-stationary over the area of interest, while the leading section moved away, eventually reaching the sea. The cell that remained over the airport started to decay in both size and intensity until completely dissipating around 14:20 UTC. This type of anomalous movements is one of the major challenges in tracking and forecasting severe thunderstorms, as they are highly dependent on internal storm dynamics [33]. Current technologies are far from detecting such processes accurately in real time. However, for the purposes of our research, if the end-user has received an accurate storm warning this weakness does not affect the final decision.

5.1.3. Bergamo Case, 6 August 2019

The thunderstorm that impacted Bergamo airport on 6 August 2019 had small dimensions, as in the Venice case (Figure 9). The major impact on the airport was reported at 18:40 UTC. The analyzed storm in Figure 9, ID65, was first identified and tracked when it was already very close to the airport, inside the area of operations. It showed quasi-stationary behavior from the beginning. This is a major challenge for operations because the response time is very short. However, the algorithm worked properly, indicating from the initial identification that the airport was about to be affected in the next few minutes. In addition, the nowcasted affected area for the next 30 min was considerably good from the beginning. Around 18:40, the storm in Figure 9 reached its maximum size and maximum DVIL intensity values. Shortly afterwards, at 18:55, the storm split and the label ID65 followed the fragment that continued to propagate to the east. In the following time steps, the storm increased its translation speed and strongly decreased in size until its dissipation after 19:35 UTC, when it was still inside the area of operations of the airport.

5.2. MODE Software for the Nowcasting Approach of SINOPTICA

For the integration of nowcasting into software for ATM, we defined three different time windows, one for each case study. This allowed us to evaluate how the ATM software reacts when ingesting slightly different predictions from the same phenomena obtained with different nowcasting methods [24]. For these time windows, RaNDeVIL was applied and the outputs (forecasted areas) were selected according to the criteria followed in the SINOPTICA project. These outputs were saved as netCDF files and MODE software was applied to evaluate the performance.

As an example, Figure 10 illustrates the study case of Milano during the period compressed between 14:25 UTC and 15:30 UTC. Nowcasting was applied for the region surrounding the airport of Malpensa between longitudes 7–10° and latitudes 45–47°. Figure 10 shows the overlap between the observed (contour) and nowcasted (blue) DVIL ($>1 \text{ g/m}^3$) areas obtained from MODE.

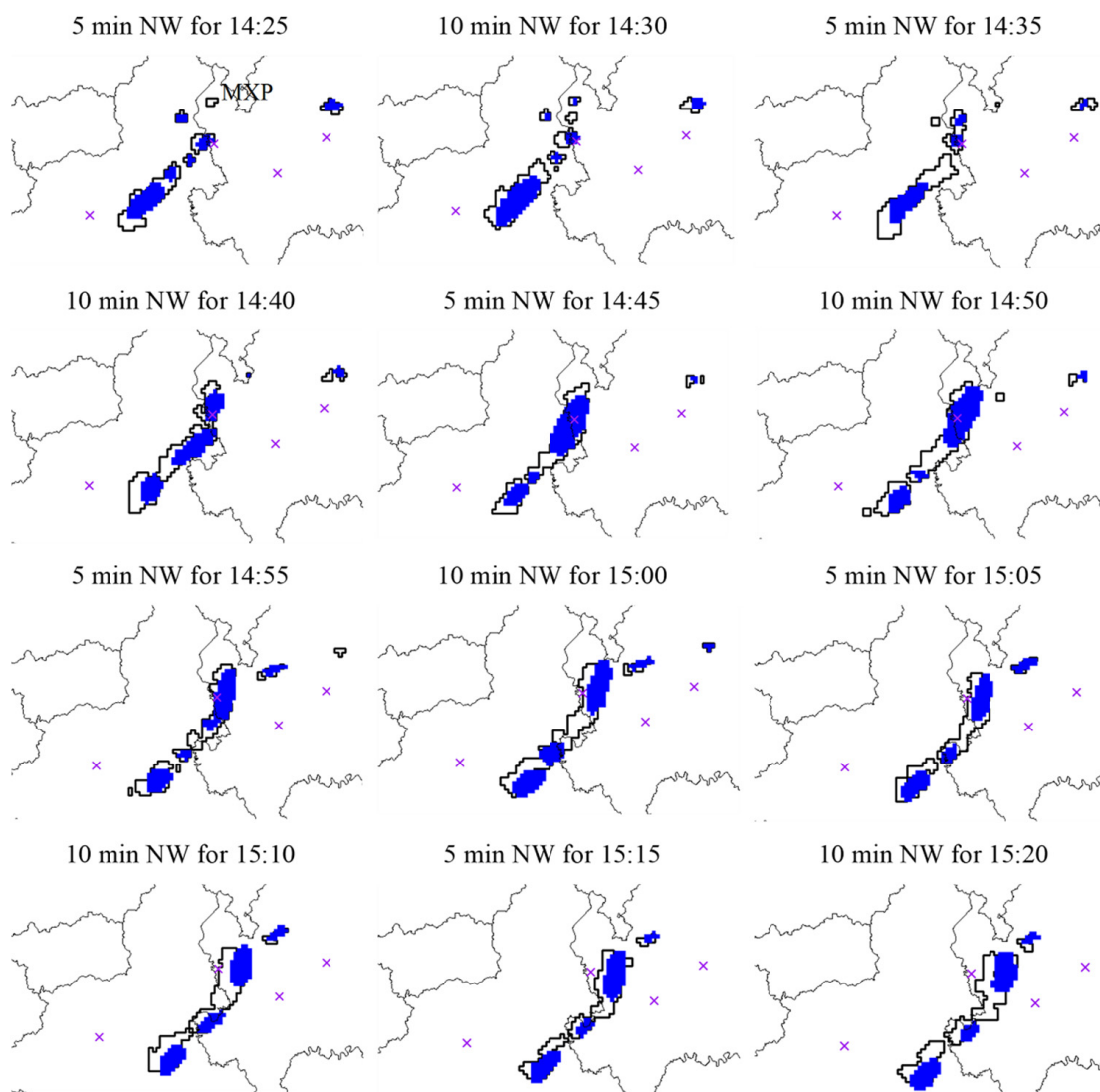


Figure 10. Comparison between observed storms (black contours) and the forecast ones for the same time by RaNDeVIL (filled blue shapes) for the Milano study case (11 May 2019). Both forecasted and observed fields are DVIL areas over 1 g/m^3 threshold. Purple crosses are the nearest airports. The Milano-Malpensa airport is labelled in the first image as MXP.

Table 1 shows the MODE indices for the different case studies (Bergamo case: 18:05–19:15 UTC; Venice case: 15:45–16 UTC). The centroid distance, area ratio, and

total interest indices are the average values obtained for the identified clusters at each time step. The total values shown in this table are obtained by the addition of the corresponding values for all the time steps.

Table 1. Cluster indices from MODE analysis for RaNDeVIL in Milano, Bergamo and Venice cases for the different analyzed periods.

RaNDeVIL Experiment	Centroid Distance [Grid Units]	Area Ratio	Total Observed Area [Grid Units]	Total Forecasted Area [Grid Units]	Intersection Area [Grid Units]	Total Interest
Milano	1.485	0.750	2532	1701	1241	0.993
Bergamo	1.278	0.611	1922	1064	884	0.974
Venice	1.060	0.618	3758	2223	1881	0.972

Overall, good scores are obtained for all the indices, with a small centroid distance, a good relation between the forecasted, observed, and intersected area, an area ratio between 0.61 and 0.75 (maximum score is 1), and a total interest index very close to 1 (maximum score). While the best scores were obtained for the Milano case, the Bergamo and Venice cases showed an underestimation of the forecasted total storm affected area, though there was good ability to locate the potential storm affected areas. The small centroid distance confirms this as well. The total interest is also close to 1, though not as good as in the Milano case.

5.3. Application of Nowcasting to Air Traffic Controller Support

For their usability in air traffic control, convection cells were converted into time-dependent 2D polygons, each with a fixed validity period. These were provided to an AMAN that assists approach controllers in organizing the airspace in the vicinity of airports as well as their surrounding sectors by suggesting approach routes, generating aircraft type-specific 4D trajectories, compiling approach sequences for each runway, and calculating overflight times for significant waypoints and runway thresholds [40]. The AMAN is adaptive, meaning that it can react to a changing traffic situation or weather conditions within a few seconds and adjust the proposed trajectories, sequences, and target times.

To test the usability and usefulness of the nowcasts, DLR's "4-Dimensional Cooperative Arrival Manager" AMAN (4D-CARMA) was extended to include Milano-Malpensa Airport [2]. In addition to the airspace structure with the standard approach routes and metering fixes, the local approach procedures had to be implemented for this purpose. The air traffic scenario selected was 11 May 2019, the Milano case, an extreme weather event that resulted in a longer closure of the airport in the afternoon as well as several flight diversions and delays. Subsequent analysis of the real traffic data from FlightRadar24, showed that average aircraft approach distances to Malpensa airport increased by 9.8% and average approach times by 12.6% due to the extreme weather compared to undisturbed traffic in normal weather situations.

For the creation of the traffic scenario, a circle with a radius of 150 nautical miles was drawn around the airport reference point as the planning horizon. For the validation traffic scenario, positions, altitudes, and times when crossing this horizon were recorded for each aircraft and adopted as initial conditions. In this way, approach traffic with its specific traffic mix in terms of aircraft types and spatial approach distribution could be modelled realistically. For representation of the traffic, the DLR internal traffic simulation ArrOS was used, which adheres very closely to the trajectory proposals of AMAN, making for a good simulation of cooperating pilots and air traffic controllers. As a comparison scenario, traffic was calculated both without weather influence and with the real weather as well as the results of the RaNDeVIL nowcasts (Figure 11).

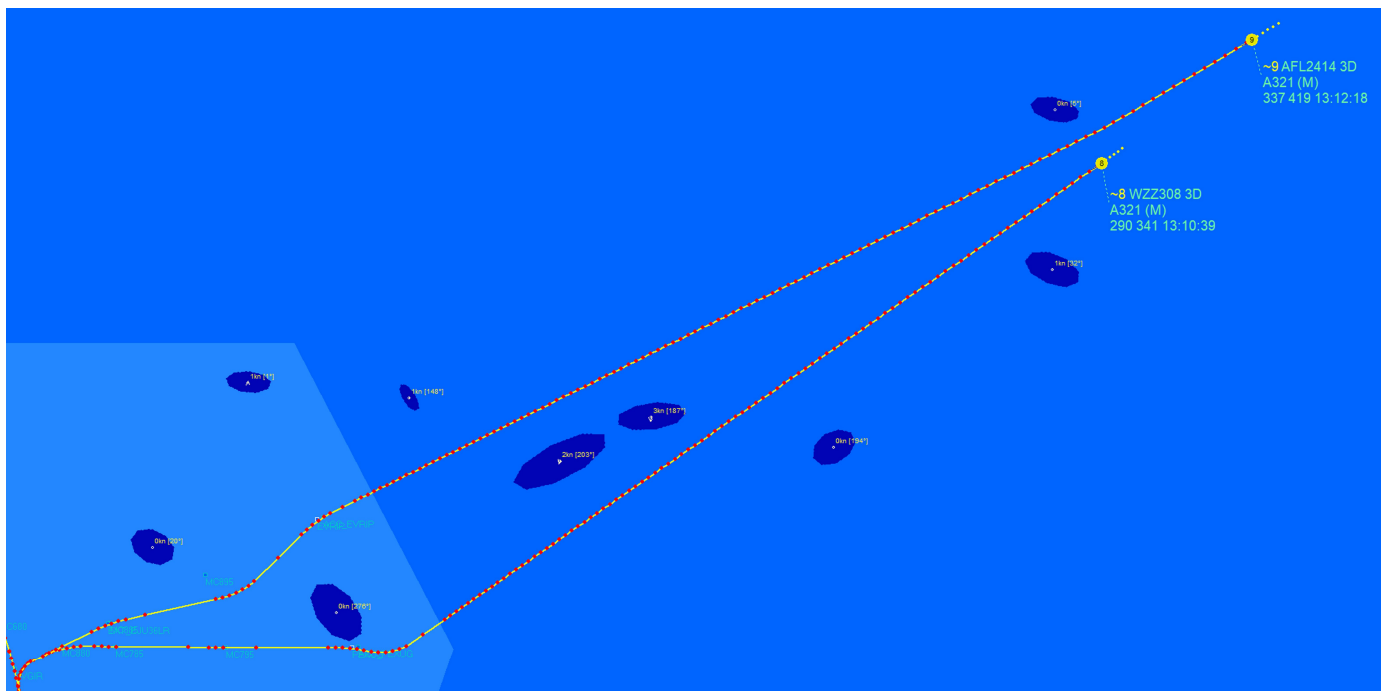


Figure 11. Examples of planned approach trajectories (yellow lines with red dots) depending on meteorologically-determined routing for the two aircraft, WZZ308 and AFL2414 (yellow circles with numbers eight and nine, indicating their actual position in the landing sequence). Although the two aircraft approaching Malpensa from the northeast are almost on the same approach route, with a time difference of only a few minutes, they are assigned significantly different routes due to the forecasted weather development (blue filled polygons) in order to take the shortest safe route to the airport. Malpensa traffic from 11 May 2019 with weather from 6 August 2019 and RaNDeVIL nowcast model.

Using the nowcasts in an AMAN, controllers can be provided with early indications of weather developments, allowing long-range diversions to be planned and implemented (Figure 11). In the traffic simulation, it was shown that in the two different weather scenarios an average increase in flight distances of only 0.49% and approach times of 1.05% would have to be accepted. Although these results are highly dependent on the particular weather event, the general traffic situation, and the airport, they show that by combining a fast and reliable weather forecasting with an air traffic controller decision support system, the meteorological impact regarding additional flight times and flight distances in the approach phase can be reduced to less than one tenth.

6. Conclusions

This paper has presented a fast and reliable method for identifying and nowcasting 2D convective cells with the potential to produce severe weather that could affect Air Traffic Management (ATM) near airports. The starting point was the premise that a very short processing methodology for identifying and nowcasting convective cells with the potential to produce severe weather is needed to support air traffic controllers. The proposal was applied to three case studies from the H2020 project SINOPTICA conducted in Italy in 2019.

Considering the aforementioned literature and previous knowledge, it was possible to develop a short-term identification, tracking, and nowcasting system for convective environments based on the VIL density radar product (DVIL). The chosen configuration of RaNDeVIL was fixed for the study area and independent of the size of the storm system. The algorithm used a DVIL intensity threshold of $R_i = 1 \text{ g/m}^3$ and a $R_s = 10$ pixels to characterize the storms as the minimum size to guarantee a storm structure. However, this configuration may need to be adjusted in order to apply the algorithm to other regions, where thunderstorms and severe weather are associated with clouds having different char-

acteristics. In the case studies, smaller thresholds dramatically increased the number of storms and the number of splitting procedures, making it difficult for the algorithm to produce a consistent direction of storm propagation. On the other hand, higher ones dramatically decreased the lifetime of the storms, impeding both the tracking and nowcasting of these storms, as storms were generated and decayed before the algorithm could track or nowcast them. To predict the behavior of storms, the algorithm characterizes them individually, taking into account the storm's past to carry out the nowcasting procedure. Another advantage of working with the DVIL product is that the algorithm is easily adaptable for any airport or convective environment that has coverage in a weather radar, while the availability of different CAPPI levels is not the same for all weather radars.

Furthermore, the results had proven that the algorithm can reliably reproduce the 3D behavior of thunderstorms for the case studies used in the SINOPTICA project. The aforementioned capabilities are crucial when air traffic controllers must make decisions in a very short time (less than a few minutes), such as the cases analyzed in this present study. When integrated into an AMAN, nowcasts can support controllers very effectively by providing routes that avoid severe weather, approach sequences, and target times to organize the traffic near airports. Our results demonstrate that the algorithm can effectively approximate future thunderstorm trajectories and the area expected to be affected by storms for the study cases in the SINOPTICA project, with especially good performance for the time horizons targeted in the project. Beyond these times, the results will probably be poorer, but can nonetheless provide valuable information to end users regarding the storm propagation direction and possible impacts in future scenarios.

This study emerged from the necessity of air traffic controllers having very-short-term, accurate, compact, and easy understandable weather forecasts to assist them in aircraft guidance during approach to an airport. End users have previously expressed the difficulties involved in properly checking the latest national weather forecasts available when severe weather phenomena occur near an airport due their high workloads. They have additionally expressed that classic 3D nowcasting products are too complex to understand under these circumstances. The developed algorithm perfectly adapts to these needs by providing nowcasting information ready to integrate into an AMAN shortly after receiving the last radar image, and the possibility of synthetic visualization of approaching storms on the air traffic control display monitor. The different possibilities of visualization and a preliminary opinion assessment by the air traffic controllers themselves is discussed in [24].

As future work, more case studies and targeting different types of adverse and severe weather that pose difficulties to ATC will be explored, as well as how long the nowcasting time horizon can be expanded while still obtaining meaningful nowcasts. Future work will additionally contemplate incorporating the tendency of the change in storm size based on the last radar product in the area extrapolation, in addition to the centroid distances. This could improve the precision of prediction without increasing the computational cost. While this is a purely graphical approach, it could be quite sufficient for integration into tactical controller support systems.

Author Contributions: Conceptualization, L.E., T.R., M.C.L., R.B., S.F., M.K., M.L., V.M., M.M., A.P., E.R. and M.-M.T.; methodology, L.E., T.R., O.G. and M.-M.T.; software, L.E.; validation, L.E. and T.R.; formal analysis, L.E.; investigation, L.E., T.R., O.G., S.F. and M.-M.T.; data curation, L.E., R.B., M.K., M.L., V.M., M.M., A.P. and E.R.; writing—original draft preparation, L.E. and T.R.; writing—review and editing, L.E., T.R., M.C.L., M.K., M.L., V.M., M.M., A.P. and M.-M.T.; visualization, L.E., T.R., O.G. and M.-M.T.; supervision, M.C.L.; project administration, A.P. All authors have read and agreed to the published version of the manuscript.

Funding: This research was funded by SESAR Joint Undertaking (JU), under the Horizon 2020 European Union research and innovation program, grant agreement No. 892362 (<https://cordis.europa.eu/project/id/892362>, accessed on 19 June 2023).

Institutional Review Board Statement: Not applicable.

Informed Consent Statement: Not applicable.

Data Availability Statement: The data from the results presented in this study are available under reasonable request from the corresponding author. Radar data are provided and managed by the Italian Civil Protection Department (DPC). Data obtained from European Severe Weather Database is available on <https://www.eswd.eu/> (accessed on 19 June 2023). Data obtained from [FlightRadar24.com](https://www.flightradar24.com) is available at <https://www.flightradar24.com/commercial-services/data-services> (accessed on 19 June 2023).

Acknowledgments: This work was carried out under the framework of the SINOPTICA (H2020-SESAR-2019-2, 892362), a European project of Horizon 2020. The authors would like to thank Italian Civil Protection for the radar data. Thanks also go to the SMC and to the CIMA for their collaboration. We acknowledge meteorologist Steven Hunter for English revision and correction.

Conflicts of Interest: Because one of the co-authors is the Guest Editor of this Special Issue, we needed to exclude this person from the decision process in order to avoid conflict of interest. The funders had no role in the design of the study; in the collection, analyses, or interpretation of data; in the writing of the manuscript; or in the decision to publish the results.

Abbreviations

4D-CARMA	Four-Dimensional Cooperative Arrival Manager
ADS-B	Automatic Dependent Surveillance—Broadcast
AMAN	Arrival Manager system
ATC	Air Traffic Control
ATM	Air Traffic Management
CAPPI	Constant Altitude Plan Position Indicator
CORTEC	Continuity Tracking Radar Echoes by Correlation
DLR	German Aerospace Center
DVIL	Density of the Vertical Integrated Liquid
ESWD	European Severe Weather Database
ETM	Echo Top Maximum
MODE	Method for Object-Based Evaluation
MPX	Malpensa airport
PPI	Plan Position Indicator
RaNDeVIL	Radar Nowcasting with Density of VIL
ROI	Region Of Interest
SCIT	Storm Cell Identification and Tracking

References

1. Reitmann, S.; Alam, S.; Schultz, M. Advanced Quantification of Weather Impact on Air Traffic Management. In Proceedings of the 13th USA/Europe Air Traffic Management Research and Development Seminar (ATM2019), Vienna, Austria, 17–21 June 2019.
2. Ohneiser, O.; Kleinert, M.; Muth, K.; Gluchshenko, O.; Ehr, H.; Gross, N.; Temme, M.-M. Bad Weather Highlighting: Advanced Visualization of Severe Weather and Support in Air Traffic Control Displays. In Proceedings of the 2019 IEEE/AIAA 38th Digital Avionics Systems Conference (DASC), San Diego, CA, USA, 8–12 September 2019. [\[CrossRef\]](#)
3. Department of the Air Force Washington DC. Weather for Aircrews. In *Air Force Handbook 11-203*; Department of the Air Force Washington DC: Washington, DC, USA, 1997; Volume 1, p. 234.
4. Esbrí, L.; Rigo, T.; Llasat, M.C.; Aznar, B. Identifying Storm Hotspots and the Most Unsettled Areas in Barcelona by Analysing Significant Rainfall Episodes from 2013 to 2018. *Water* **2021**, *13*, 1730. [\[CrossRef\]](#)
5. Rigo, T.; Llasat, M.C.; Esbrí, L. The Results of Applying Different Methodologies to 10 Years of Quantitative Precipitation Estimation in Catalonia Using Weather Radar. *Geomatics* **2021**, *1*, 347–368. [\[CrossRef\]](#)
6. Kalchikhin, V.V.; Kobzev, A.A. Use of an optical rain gauge in a system of monitoring severe weather phenomena. *IOP Conf. Ser. Earth Environ. Sci.* **2018**, *211*, 012063. [\[CrossRef\]](#)
7. Andrieu, H.; Creutin, J.D.; Delrieu, G.; Faure, D. Use of a weather radar for the hydrology of a mountainous area. Part I: Radar measurement interpretation. *J. Hydrol.* **1997**, *193*, 1–25. [\[CrossRef\]](#)
8. Harrison, D.L.; Driscoll, S.J.; Kitchen, M. Improving precipitation estimates from weather radar using quality control and correction techniques. *Meteorol. Appl.* **2000**, *7*, 135–144. [\[CrossRef\]](#)
9. Ye, B.Y.; Lee, G.W.; Park, H.M. Identification and removal of non-meteorological echoes in dual-polarization radar data based on a fuzzy logic algorithm. *Adv. Atmos. Sci.* **2015**, *32*, 1217–1230. [\[CrossRef\]](#)
10. Heymsfield, G.M.; Ghosh, K.K.; Chen, L.C. An interactive system for compositing digital radar and satellite data. *J. Clim. Appl. Meteorol.* **1983**, *22*, 705–713. [\[CrossRef\]](#)

11. Rigo, T.; Farnell, C. Using maximum Vertical Integrated Liquid (VIL) maps for identifying hail-affected areas: An operative application for agricultural purposes. *Tethys* **2019**, *16*, 15–24. [[CrossRef](#)]
12. Wilson, J.W.; Crook, N.A.; Mueller, C.K.; Sun, J.; Dixon, M. Nowcasting Thunderstorms: A Status Report. *Bull. Am. Meteorol. Soc.* **1998**, *79*, 2079–2099. [[CrossRef](#)]
13. Dixon, M.; Wiener, G. TITAN: Thunderstorm Identification, Tracking, Analysis, and Nowcasting—A Radar-based Methodology. *J. Atmos. Ocean. Technol.* **1993**, *10*, 785–797. [[CrossRef](#)]
14. Johnson, J.T.; MacKeen, P.L.; Witt, A.; Mitchell, E.D.; Stumpf, G.J.; Eilts, M.D.; Thomas, K.W. The storm cell identification and tracking algorithm: An enhanced WSR-88D algorithm. *Weather. Forecast.* **1998**, *13*, 263–276. [[CrossRef](#)]
15. Kyznarová, H.; Novák, P. CELLTRACK—Convective cell tracking algorithm and its use for deriving life cycle characteristics. *Atmos. Res.* **2009**, *93*, 317–327. [[CrossRef](#)]
16. Bellon, A.; Zawadzki, I.; Kilambi, A.; Lee, H.C.; Lee, Y.H.; Lee, G. McGill algorithm for precipitation nowcasting by lagrangian extrapolation (MAPLE) applied to the South Korean radar network. Part I: Sensitivity studies of the Variational Echo Tracking (VET) technique. *Asia-Pacific J. Atmos. Sci.* **2010**, *46*, 369–381. [[CrossRef](#)]
17. Atencia, A.; Kann, A.; Wang, Y.; Meier, F. Localized variational blending for nowcasting purposes. *Meteorol. Zeit* **2020**, *29*, 247–261. [[CrossRef](#)]
18. del Moral, A.; Rigo, T.; Llasat, M.C. A radar-based centroid tracking algorithm for severe weather surveillance: Identifying split/merge processes in convective systems. *Atmos. Res.* **2018**, *213*, 110–120. [[CrossRef](#)]
19. Chandrasekar, V. AI in Weather Radars. In Proceedings of the 2020 IEEE Radar Conference (RadarConf20), Florence, Italy, 21–25 September 2020; pp. 1–3. [[CrossRef](#)]
20. Zhou, K.; Zheng, Y.; Dong, W.; Wang, T. A Deep Learning Network for Cloud-to-Ground Lightning Nowcasting with Multisource Data. *J. Atmos. Ocean. Technol.* **2020**, *37*, 927–942. [[CrossRef](#)]
21. Woo, W.C.; Wong, W.K. Operational Application of Optical Flow Techniques to Radar-Based Rainfall Nowcasting. *Atmosphere* **2017**, *8*, 48. [[CrossRef](#)]
22. Lin, H.H.; Tsai, C.C.; Liou, J.C.; Chen, Y.C.; Lin, C.Y.; Lin, L.Y.; Chung, K.S. Multi-Weather Evaluation of Nowcasting Methods Including a New Empirical Blending Scheme. *Atmosphere* **2020**, *11*, 1166. [[CrossRef](#)]
23. Rubnich, M.; Delaura, R. An Algorithm to Identify Robust Convective Weather Avoidance Polygons in En Route Airspace. In Proceedings of the 10th AIAA Aviation Technology, Integration, and Operations (ATIO) Conference, Fort Worth, TX, USA, 13–15 September 2010; p. 9164. [[CrossRef](#)]
24. Temme, M.-M.; Gluchshenko, O.; Nöhren, L.; Kleinert, M.; Ohneiser, O.; Muth, K.; Ehr, H.; Groß, N.; Temme, A.; Lagasio, M.; et al. Innovative Integration of Severe Weather Forecasts into an Extended Arrival Manager. *Aerospace* **2023**, *10*, 210. [[CrossRef](#)]
25. Vulpiani, G.; Pagliara, P.; Negri, M.; Rossi, L.; Gioia, A.; Giordano, P.; Alberoni, P.; Cremonini, R.; Ferraris, L.; Marzano, F.S. The Italian Radar Network within the National Early-Warning System for Multi-Risks Management. In Proceedings of the Fifth European Conference on Radar in Meteorology and Hydrology, Helsinki, Finland, 30 June–4 July 2008.
26. Edwards, R.; Thompson, R.L. Nationwide comparisons of hail size with WSR-88D vertically integrated liquid water and derived thermodynamic sounding data. *Weather Forecast.* **1998**, *13*, 277–285. [[CrossRef](#)]
27. Groenemeijer, P.; Púčik, T.; Holzer, A.M.; Antonescu, B.; Riemann-Campe, K.; Schultz, D.M.; Kühne, T.; Feuerstein, B.; Brooks, H.E.; Doswell, C.A.; et al. Severe Convective Storms in Europe: Ten Years of Research and Education at the European Severe Storms Laboratory. *Bull. Am. Meteorol. Soc.* **2017**, *98*, 2641–2651. [[CrossRef](#)]
28. Rigo, T.; Carmen Llasat, M. Forecasting hailfall using parameters for convective cells identified by radar. *Atmos. Res.* **2016**, *169*, 366–376. [[CrossRef](#)]
29. Qi, Y.; Zhang, J.; Zhang, P. A real-time automated convective and stratiform precipitation segregation algorithm in native radar coordinates. *Q. J. R. Meteorol. Soc.* **2013**, *139*, 2233–2240. [[CrossRef](#)]
30. Seo, B.-C.; Krajewski, W.F.; Qi, Y. Utility of Vertically Integrated Liquid Water Content for Radar-Rainfall Estimation: Quality Control and Precipitation Type Classification. *Atmos. Res.* **2020**, *236*, 104800. [[CrossRef](#)]
31. Rigo, T.; Llasat, M.C. A methodology for the classification of convective structures using meteorological radar: Application to heavy rainfall events on the Mediterranean coast of the Iberian Peninsula. *Nat. Hazards Earth Syst. Sci.* **2004**, *4*, 59–68. [[CrossRef](#)]
32. del Moral, A.; del Carmen Llasat, M.; Rigo, T. Connecting flash flood events with radar-derived convective storm characteristics on the northwestern Mediterranean coast: Knowing the present for better future scenarios adaptation. *Atmos. Res.* **2020**, *238*, 104863. [[CrossRef](#)]
33. López, L. Convección Atmosférica Severa: Pronóstico e Identificación de Tormentas de Granizo. Ph.D. Thesis, Universidad de León, León, Spain, 2003; p. 207.
34. Ceperuelo, M.; Llasat, M.C.; López, L.; García-Ortega, E.; Sánchez, J.L. Study of 11 September 2004 hailstorm event using radar identification of 2-D systems and 3-D cells. *Adv. Geosci.* **2006**, *7*, 215–222. [[CrossRef](#)]
35. Davis, C.; Brown, B.; Bullock, R. Object-based verification of precipitation forecasts. Part I: Methodology and application to mesoscale rain areas. *Mon. Weather Rev.* **2006**, *134*, 1772–1784. [[CrossRef](#)]
36. Brown, B.G.; Gotway, J.H.; Bullock, R.; Gilleland, E.; Fowler, T.; Ahijevych, D.; Jensen, T. The Model Evaluation Tools (MET): Community Tools for Forecast Evaluation. In Proceedings of the 25th Conference on International Interactive Information and Processing Systems (IIPS) for Meteorology, Oceanography, and Hydrology, Phoenix, AZ, USA, 10 January 2009; Volume 9, p. 6.

37. Newman, K.; Opatz, J.; Jensen, T.; Prestopnik, J.; Soh, H.; Goodrich, L.; Brown, B.; Bullock, R.; Halley Gotway, J. *The MET Version 10.1.2 User's Guide*. Developmental Testbed Center. 2022. Available online: <https://github.com/dtcenter/MET/releases> (accessed on 19 June 2023).
38. Davis, C.; Brown, B.; Bullock, R. Object-based verification of precipitation forecasts. Part II: Application to convective rain systems. *Mon. Weather Rev.* **2006**, *134*, 1785–1795. [[CrossRef](#)]
39. Mazzarella, V.; Milelli, M.; Lagasio, M.; Federico, S.; Torcasio, R.C.; Biondi, R.; Realini, E.; Llasat, M.C.; Rigo, T.; Esbri, L.; et al. Is an NWP-Based Nowcasting System Suitable for Aviation Operations? *Remote Sens.* **2022**, *14*, 4440. [[CrossRef](#)]
40. Harwood, K.; Sanford, B.D.; Lee, K.K. Developing ATC Automation in the Field: It Pays to Get Your Hands Dirty. *Air Traffic Control Q.* **1998**, *6*, 45–70. [[CrossRef](#)]

Disclaimer/Publisher's Note: The statements, opinions and data contained in all publications are solely those of the individual author(s) and contributor(s) and not of MDPI and/or the editor(s). MDPI and/or the editor(s) disclaim responsibility for any injury to people or property resulting from any ideas, methods, instructions or products referred to in the content.